Exp Fluids (2007) 43:779–797
DOI 10.1007/s00348-007-0346-7

RESEARCH ARTICLE

Flapping flexible fish

Periodic and secular body reconfigurations in swimming lamprey, *Petromyzon marinus*

Robert G. Root · Hayden-William Courtland · William Shepherd · John H. Long Jr

Received: 22 January 2007 / Revised: 5 June 2007 / Accepted: 11 June 2007 / Published online: 13 July 2007

Abstract In order to analyze and model the body kinematics used by fish in a wide range of swimming behaviors, we developed a technique to separate the periodic whole-body motions that characterize steady swimming from the secular motions that characterize changes in whole-body shape. We applied this harmonic analysis technique to the study of the forward and backward swimming of lamprey. We found that in order to vary the unsteadiness of swimming, lamprey superimpose periodic and secular components of their body motion, modulate the patterns and magnitudes of those components, and change shape. These kinematic results suggest the following hydromechanical hypothesis: steady swimming is a maneuver that requires active suppression of secular body reconfigurations.

R. G. Root (✉)
Mathematics Department, Lafayette College,
Easton, PA 18042, USA
e-mail: robroot@lafayette.edu

H.-W. Courtland
Department of Orthopaedics,
Mount Sinai School of Medicine,
New York, NY 10029, USA

W. Shepherd
Steinhart Aquarium, California Academy of Sciences,
San Francisco, CA 94118, USA

J. H. Long Jr
Biology Department and Interdisciplinary
Robotics Research Laboratory, Vassar College,
Poughkeepsie, NY 12604, USA
e-mail: jolong@vassar.edu

1 Introduction

Fish bodies are internally-actuated flapping foils that generate flexures to produce, augment, and modulate momentum transfer to and from body and water. In so doing, fish not only generate thrust, but they also create a range of mechanical behaviors, from constant-velocity cruising to high-acceleration startle responses and straight-line translation to rotational maneuvers. The dynamics of coupled internal and external forces, i.e., the hydroelastic system, reveal themselves in a body's instantaneous kinematic configuration and reconfiguration over time (Bowtell and Williams 1993; Cheng et al. 1998; Daniel and Tu 1999; Daniel and Coombes 2002). For biologists and engineers studying biological flow, accurate body kinematics are essential (1) to determine general features of locomotor kinematics across behaviors and species, (2) as input for open-loop models that estimate dynamics of the coupled hydroelastic system (Hess and Videler 1984), and (3) for validation of motions output by closed-loop hydroelastic models (Carling et al. 1998; Cheng and Blickhan 1993). The first of these pursuits, determination of general features, is the focus of this paper. In particular, our goal is to quantify body kinematics in such a way as to permit fine-scale temporal and spatial description, within a single cycle and for the whole body, respectively, and at the same time, to discover new ways of characterizing the kinematics of the whole body.

From a biological point of view, we seek to analyze, discriminate among, and generalize from a group of swimming behaviors showing high kinematic variation: translational swimming (1) at speeds determined by the animal rather than the investigator, (2) in forward and backward directions within the fish's frame of reference and using the same propulsive mechanism, and (3) of only a single or few

propulsive cycles. Variation in swimming speed occurs naturally even in fish migrating upstream, a situation that might appear to demand constant-velocity swimming; individuals vary speed, by modulating the kinematic properties of cycle frequency and lateral body amplitudes, to negotiate flow obstacles inherent in natural hydrology (Castro-Santos 2005). Further, variation in swimming kinematics is higher in lake sturgeon that select their own swimming speeds compared with those for whom speed is determined by the investigator (Webb 1986). Also, kinematic variations in white sturgeon selecting their own speeds include changes in body shape, with individuals swimming at the same speeds at different times selecting different magnitudes of body curvature (Long 1995). Finally, drastic variation in swimming kinematics of European eels is seen between forward and backward undulatory swimming, where, at similar speeds, the body has different shape configurations and kinematic patterns (D'Aout and Aerts 1999).

In experimental situations, kinematic variations during swimming are often carefully minimized. For "steady" translational swimming, one such approach is to analyze only those trials in which the speed over three to five sequential tail-beat cycles varies by a small and predeterimined magnitude (D'Aout and Aerts 1999; Jayne and Lauder 1995; Tytell 2004b). For trials meeting these conditions, points along the body's midline, from snout to tail tip, are tracked through time. From the many possible metrics, tail-beat frequency (Hz) and lateral tail-beat amplitude are considered fundamental, as shown by their use in important dimensionless numbers such as the Strouhal number (Taylor et al. 2003; Triantafyllou et al. 1993), Froude efficiency (see Blickhan and Cheng 1994), and the wake vortex ratio (Dabiri 2005) for power and thrust approximations based on Lighthill's classic elongated body theory (Lighthill 1975; Wu 1977; Webb 1975). This focus on the tail-beat frequency and amplitude are justified because, in undulatory swimmers, the tail is a trailing edge and, therefore, a site of vortex shedding. At the same time, vortex production is a whole-body phenomenon, as demonstrated by oscillating pressure differentials on the flapping flexible body (Liu et al. 1996; Long et al. 2002) and direct visualization of circulation developed on the body (Tytell 2004a, b; Müller and van Leeuwen 2004). If it is the case that the whole body is a flapping foil involved in thrust production, we predict that new kinematic features of the whole body can be discovered that will help us to understand the mechanics of highly variable swimming behaviors.

Creating a method that mathematically decomposes the whole-body kinematics of lamprey swimming forward and backward at speeds of their own choosing, we address the following specific questions. First, how "steady" is steady swimming, where "steady" refers to the purely periodic nature of the undulatory motions? Second, if we measure and characterize undulatory motion as a multi-dimensional matrix of periodic and secular components, what aspects of this matrix are modulated in order to alter performance and behavior? Third, given reports, mentioned above, of fish changing body shape, what we call "reconfiguration", do fish reconfigure differently in different situations?

2 Methods

2.1 Experimental animals

We chose an elongate-body swimmer, the marine lamprey, *Petromyzon marinus*, as our study species for several reasons. First, they swim forward and backward using traveling waves of body flexure (Islam et al. 2006). While they swim forward routinely, when provoked lamprey retract their heads, as most elongate swimmers do (Ward and Azizi 2001), and swim backward with body kinematics in between the excellent backward propulsion of eels (D'Aout and Aerts 1999) and the stationary motion of ropefish (Bierman et al. 2004). Since in both swimming directions lamprey use traveling body flexures, they provide us with a wide range of swimming behaviors and body reconfigurations without the complications of comparing different species. Second, much is known about the underlying neural control of lamprey swimming, since they are used as a model organism for the neural control of vertebrate locomotion in general (Grillner et al. 1995; Grillner 1996; Ijspeert 2001; Sigvardt 1989; Guan et al. 2001) and eel-like swimming in particular (Carling et al. 1998; Ekeberg 1993; Ijspeert et al. 1999; Lighthill 1975; Williams et al. 1998). Third, lamprey have been used as the biological model for the simulation of the evolution of locomotor control systems (Ijspeert and Kodjabachian 1999; Or et al. 2002) and the design of aquatic robots (Arena et al. 2006; Crespi and Ijspeert 2006; Lachat et al. 2006).

2.2 Experimental conditions

Using high-speed video, we filmed lamprey swimming forward and backward in a still-water tank. For analysis, we biased selection of trials towards those appearing on slow-motion video to be of nearly constant velocity. We did so in order to test the ability of our methodology to detect deviations from constant velocity swimming. Since backward swimming is in part a head-retraction startle response (Ward and Azizi 2001), we also sought to measure changes in the body shape, or what we call "reconfiguration", as separate from propulsive body movements. Thus steady swimming with a constant body shape is the starting point for our analysis.

Seven metamorphosed, parasitic-phase sea lamprey, *Petromyzon marinus*, between 10 and 17 cm total length, were obtained from the Lake Huron Biological Station in Millersburg, Michigan and the Conte Anadromous Fish Research Center in Amherst, Connecticut. All lamprey were housed at 20°C in an 80 L aquarium. Swimming sequences were captured at 500 frames per second with high speed video (Kodak Ektapro model 1000 EM). The ventral surface of fish was filmed during forward and backward swimming through the glass bottom of an aquarium evenly backlit by a diffuser illuminated with a 500 W halogen light. A 10 × 10 cm square grid was placed in the video field for calibration. Swimming was initiated by gently stimulating the rostral or caudal end of the fish with a rubber tipped rod.

2.3 Digitizing and preprocessing video

Video sequences were digitized using a video deck (Sony SVO-9500MD SVHS) linked to a Macintosh IIfx computer. An *xy*-coordinate grid was overlaid upon the video screen (Image 1.51 software, Televeyes Pro video overlay board, Digital Vision, Inc.). A series of 20 points on the fish's midline was manually plotted for 20 frames per putative tailbeat cycle. These data were processed using software introduced by Jayne and Lauder (1993) to create a dataset consisting of time series of positions in two dimensions for specific points uniformly spaced on the midline of the fish. Each time series includes one pair of coordinates for each frame of the digitized video that was processed. We tracked 31 body points, extending from the rostral tip to the caudal tip. The elapsed time between successive frames was constant and is referred to as the interframe time. Since not every frame of the original video was digitized, and the number of frames skipped varies from trial to trial, the interframe time varies as well. The data form doubly indexed coordinate pairs, $\mathbf{x}_{ij} = (x_{ij}, y_{ij})$, in units of centimeters, with $1 \le i \le N$ and $0 \le j \le 30$. The index i varies over the N digitized frames, and j varies over the 31 body points.

2.4 Identifying velocity and cycle period

Following Weihs and Webb (1983), steady swimming is when the fish's undulatory motion is repetitive and the fish is moving *on average* along a straight trajectory. We regard a steadily swimming fish as having a characteristic period, p, associated with its motion. While p is traditionally measured to as the tail-beat period, taken from a single point, we define p as the *whole body cycle period*, since, for archetypal steady swimming, at the end of a cycle period the *entire* fish's body returns to its original physical configuration. This terminology is meant to signal the more balanced origin of this statistic by contrasting with the more usual tailbeat period used commonly in the biological literature.

Consider motion of a single body point of the fish. Labeling this point's position in space at one instant as $\mathbf{x}_{\text{init}}$, and the point's position after a time interval p has passed $\mathbf{x}_{\text{final}}$, the average velocity of that body point over that cycle period is

$$\mathbf{v} = \frac{\mathbf{x}_{\text{final}} - \mathbf{x}_{\text{init}}}{p}. \tag{1}$$

Steady swimming postulates that this average velocity vector, $\mathbf{v}$, and p, are constant as both the initial instant and the choice of point on the fish vary.

In current practice, tailbeat period is determined by identifying two frames in which the trailing tip is in the same relative position, for instance full extension to the fish's left, and calculating the elapsed time. While this general approach gives a good rough estimate to p, there are two important limits to its accuracy. First, it uses position information from a single point to infer a critical parameter in the kinematics of the entire fish. Given that we have position data for the entire fish, it is reasonable to seek a statistical method to use all of it to ascertain p, or equivalently its reciprocal, the *whole body cycle frequency* f. The second limitation is that determining the two frames in which the trailing tip is in the same relative position depends upon an estimation of the direction of motion of the fish, or the average velocity described above. This determination is typically done by eye, and therefore is not as accurate as a statistical technique, and this inaccuracy is particularly large in the still water situation of the data examined in this paper. Further, analysis of our kinematic data shows that both the average velocity and the period of motion display variability over the length of the fish, and so in general these quantities need to be calculated statistically. We present two techniques in this section: one based on the raw data in the time domain, and the other on data transformed to the frequency domain. The former is the natural means for estimating p, and the latter is the same for estimating f. In both cases it is essential to estimate the average velocity in conjunction with the cycle length.

2.4.1 *Estimating a cycle period and velocity in the time domain*

While standard techniques exist for identifying the periodic and long-term trends in time series data (see Brockwell and Davis 1996, Chap. 1), they are of limited use here because of the short duration of the times series relative to p. Few of our trials have two full cycles, whereas traditional methods work best when at least three cycles of data are available

(see Chatfield 2004, p 27), a point widely acknowledged in the literature on steady swimming (e.g., Jayne and Lauder 1995).

To overcome this difficulty, beginning with a dataset as described in Sect. 2.3, and taking all intervals of the specified length $p = k\Delta t$, where Δt is the interframe time for this dataset, we compute $31(N - k)$ sample average velocities, $(\mathbf{x}_{(i+k)j} - \mathbf{x}_{ij})/k\Delta t = \mathbf{v}_{ij}$. The sample mean $\hat{\mathbf{v}}_{\text{ave}}$ is henceforth called *composite average velocity*, to indicate that it is the mean of the average velocities of all body points, and distinguish it from the average velocity for individual body points, which will play an important role in the model constructed here. We compute a standard error under the unrealistic assumption that the estimates $\mathbf{v}_{ij}$ are independent via

$$\mathrm{SE}(k) = \sqrt{\frac{\sum_{i,j} |\mathbf{v}_{ij} - \mathbf{v}(k)|^2}{62(N-k)[62(N-k)-1]}}. \tag{2}$$

where $\mathbf{v}(k)$ is the composite average velocity for a lag of k, a candidate for $\hat{\mathbf{v}}_{\text{ave}}$. In contrast to autocorrelation coefficients, which—as one would expect—vary erratically over body length and lag h, this standard error varies smoothly and offers a simple algorithm for finding p and $\hat{\mathbf{v}}_{\text{ave}}$. If $\mathrm{SE}(k)$ achieves a local minimum at some $1 \le k \le N - 1$, then we assign $p = k\Delta t$ and $\hat{\mathbf{v}}_{\text{ave}} = \mathbf{v}(k)$. One of our trials has more than one local minimum, but this is because the trial is one of two with more than two full cycles. In this case, we use the shorter of the two intervals corresponding to a local minimum as p. If there is no local minimum, then $\mathrm{SE}(k)$ is monotonically decreasing for $1 \le k \le N$, and we turn to the frequency domain. In practice, this occurs in instances when p is only slightly shorter than the trial's full time interval, and the motion is not very steady, according to the criterion we develop below.

Our rationale for making the standard error rather than the sample variance our objective function is that it penalizes longer candidate p values to compensate for smaller sample sizes. Sample variance is often a monotone decreasing function unless the motion is quite steady and the trial's full interval is substantially longer than p.

2.4.2 *Estimating an average cycle frequency and velocity in the frequency domain*

To deal with instances when p is nearly as long as the trial interval in moderately to very unsteady motion, we have constructed a second technique that estimates $f = 1/p$ by applying a discrete Fourier transform that converts the data described in Sect. 2.3 to the frequency domain. The cycle frequency for each point in each dimension is then estimated, and a weighted average cycle frequency is computed. The computation involves three steps.

First, we compute a *windowed discrete Fourier transform* (henceforth FT) of the x- and y-components for the positions for each individual point. The window is a frequency bandwidth that extends from zero to twice the frequency associated with a low estimate of f. This filters out frequencies from harmonics of the estimated tailbeat frequency. The windowing serves two purposes: it aids in filtering out the displacement from the FT, and it excludes interference from the first harmonic in determination of f.

Second, we filter the net displacement of each body point out of its FT by least-squares regression. Performing this in a low-frequency window is critical for the technique's accuracy. If regression is performed in the time domain, the result is less accurate estimates of the body point's velocity, $\mathbf{v}$, and of p. From the net displacements in each coordinate an average velocity vector, $\mathbf{v}_j$ is derived for each body point. These are averaged with equal weighting to give $\hat{\mathbf{v}}_{\text{ave}}$. The residuals of this regression are a filtered FT (henceforth fFT), and this represents the frequency profile of the periodic portion of the motion of the body point. A periodogram shows the amplitude data for this frequency profile, for both spatial coordinates of all 31 body points in a representative dataset (Fig. 1).

Third, each body point offers two estimates of f, the maximum amplitude frequency in the fFT in each spatial dimension. These are denoted $f_{x,i}$ and $f_{y,i}$, where the index i varies over body points. The amplitudes at these frequencies, denoted $a_{x,i}$ and $a_{y,i}$ are used to weight the average of the frequencies over body points and directions to compute f. That is,

$$f = \frac{\sum_{\text{bodypoints}} a_{xf_x + a_y f_y}}{\sum_{\text{bodypoints}} a_x + a_y}. \tag{3}$$

Computations demonstrate that motion in the lateral direction is dominated by the fundamental frequency of the motion, with an amplitude proportional to the flexion of the spinal chord/curvature of the notochord. The motion in the axial direction is dominated by the first harmonic, with an amplitude proportional to the square of the flexion/curvature. Since flexion is less than one, this amplitude is smaller than that in the lateral direction. Thus, if the dataset happens to have the lateral and axial directions roughly aligned with the coordinate directions, it is possible the axial direction will generate false estimates of the fundamental, off by a factor of two. Hence we set the bandwidth window to exclude the first harmonic.

The estimate for p is the reciprocal of f rounded to the nearest multiple of the interframe time, so all estimates for p are integer multiples of the interframe time.

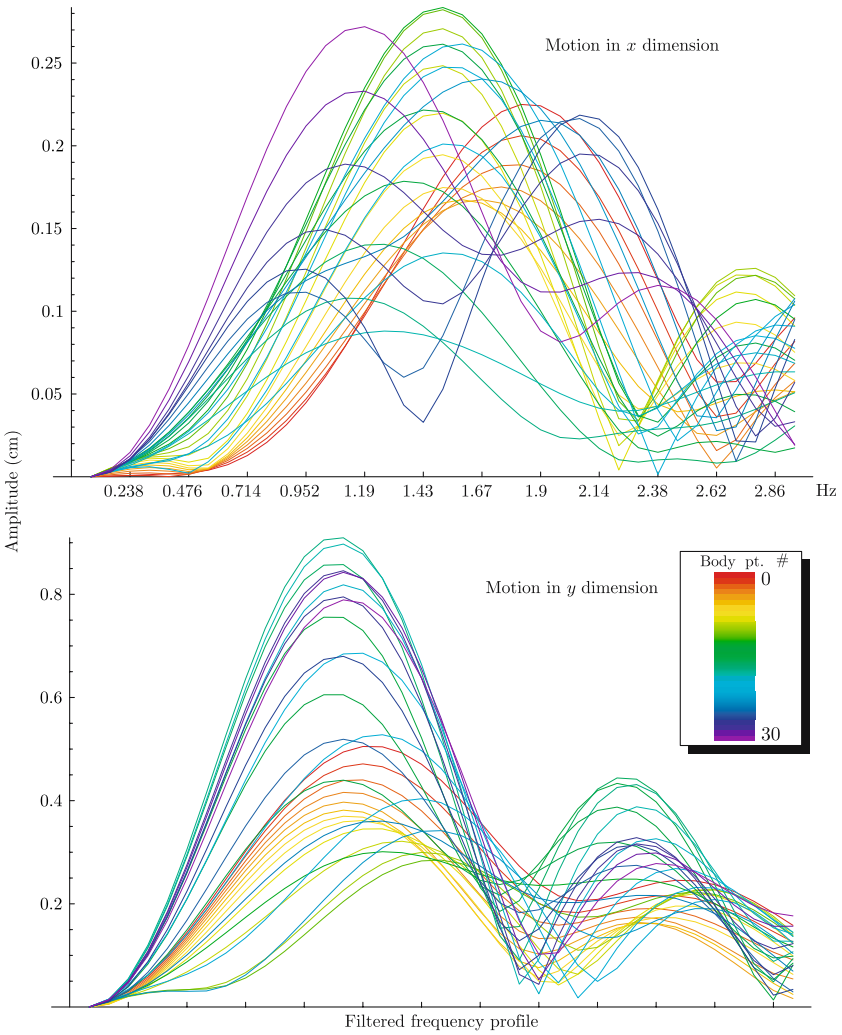

Fig. 1 Periodograms for fFT's for all body points for a representative trial where p (0.84 s or f = 1.19 Hz) was determined in the frequency domain. The frequency components due to translation, including any constant (0 Hz) component, have been eliminated from the profiles by regression. The large disparity in peaks of the various curves indicates that the different body points are displaying different fundamental frequencies. Note that while the scales in the horizontal direction are the same, the vertical scales are different, reflecting the larger amplitude of motion in the y-direction. This fish is swimming leftward in a direction roughly 20° above horizontal, as shown in Fig. 3, the trial on the *lower right*

2.5 Assessing the steadiness of swimming

Once p and $\hat{\mathbf{v}}_{\text{ave}}$ have been estimated, we can test our assumption that the swimming motion is steady. To do so, we offer an *unsteadiness index* (UI) to measure the deviation of the observed data from the ideal of steady swimming. The UI is related to, but purposely slightly different from, the standard error SE(k) minimized to find the time domain estimate of p.

The UI for a dataset with estimates of $\hat{\mathbf{v}}_{\text{ave}}$ and p is a dimensionless figure of merit quantifying the accuracy of the assumption that the dataset represents steady swimming with the specified period and velocity. Thus smaller UIs indicate more nearly steady datasets. We assume that $p = k\Delta t$ with k an integer, but this assumption can be relaxed without difficulty.

The first step in computing the UI is to compute all possible *reconfiguration errors* (RE), the relative errors between $\hat{\mathbf{v}}_{\text{ave}}$ and the average velocity of body points over a cycle. For each body point we have time series of x- and y-coordinates; a time series of position vectors for the body point, $\mathbf{x}_1, \mathbf{x}_2, \mathbf{x}_3, \ldots \mathbf{x}_N$. Compute the average velocity of the body point over the whole body cycle period that begins in frame i and ends in frame $i + k$. From Eq. 1 this gives us

$$\mathbf{v}_{\text{actual},i} = \frac{\mathbf{x}_{i+k} - \mathbf{x}_i}{p},$$

which we compare with $\hat{\mathbf{v}}_{\text{ave}}$ to get the RE

$$\text{RE}_i = \frac{\mathbf{v}_{\text{actual},i} - \hat{\mathbf{v}}_{\text{ave}}}{|\hat{\mathbf{v}}_{\text{ave}}|}. \tag{4}$$

REs are vectors that are useful in themselves in assessing the steadiness of a dataset (see Fig. 7).

Once the REs have been computed for every available cycle for every body point, we use them to compute the UI. Since the REs would all be zero for a perfectly steady swimmer, the UI is a weighted standard deviation of the REs, using the zero vector as the center value. The formula for the computation is

$$\mathrm{UI} = \sqrt{\frac{\sum_{31\ \text{points}\ \&\ 1 \le i \le N-k} |\mathrm{RE}_i|^2 \frac{|\hat{\mathbf{v}}_{\mathrm{ave}}|}{|\mathbf{v}_{\mathrm{actual},i}|}}{31(N-k)-1}}. \quad (5)$$

Note that the ratio of lengths of velocity vectors in this formula would not appear in the usual standard deviation calculation. Because the quantity $|\mathrm{RE}_i|^2$ includes a factor of $|\hat{\mathbf{v}}_{\mathrm{ave}}|^2$ in the denominator, multiplying by the ratio of lengths places the product $|\hat{\mathbf{v}}_{\mathrm{ave}}||\mathbf{v}_{\mathrm{actual},i}|$ in the denominator, giving both estimated and the computed average velocity vector weight in assessing the relative size of the error.

2.6 Modeling steady undulatory motion

The data are rotated so that the composite average velocity vector points in the positive x-direction, and each frame of the data is translated horizontally in the negative x-direction by the displacement predicted the estimated speed of the fish. That is, if $s = |\hat{\mathbf{v}}_{\mathrm{ave}}|$ in units of centimeters per interframe time, the ith frame of rotated data is translated to the left by $(i - 1)s$. The result is data that are on average stationary, assuming that $\hat{\mathbf{v}}_{\mathrm{ave}}$ is an accurate estimate. These data preserve the periodic portion of the motion, and the deviation from steadiness, including periodic axial acceleration and deceleration. The horizontal direction is now the axial direction, labeled u, and the vertical direction is now the lateral direction, labeled v.

Any function $u(t)$ with period p that is continuous and piecewise smooth (technical conditions that kinematic data always satisfy) can be written as a Fourier series (see, e.g., Tolstov 1962):

$$u(t) = u_0 + \sum_{n=0}^{\infty} A_n \cos((n+1)\omega t - \phi_n). \quad (6)$$

The quantity ω is the *fundamental angular frequency*, $\omega = 2\pi/p$. The integer multiples of the fundamental frequency $n\omega$ are the harmonics of the fundamental with the integer $n + 1$ giving the nth harmonic. Each frequency has two associated parameters that collectively characterize the function u; they are the amplitude A_n and the phase angle ϕ_n. The constant u_0 is the average value of $u(t)$.

We truncate the infinite series no later than the fourth harmonic since we can expect our discrete data to provide us with information for the first few harmonics of the full frequency spectrum. The choice of the fourth harmonic as the final term in our series is heuristic; it rarely plays a substanial role in any of our models. In practice an unmodified finite Fourier series gives a relatively poor fit to the data, even if the UI is fairly low, because, over the course of a cycle, the final configuration of the fish is never identical with its initial configuration. Even fairly steady swimmers experience changes in configuration that typically result in relative errors in their average velocity of 10% (Fig. 7). To account for this deviation from steadiness, we introduce a term that varies *secularly*. For most data sets it is sufficient to include only a constant velocity term, giving a *linearly displaced Fourier series* of this form:

$$u(t) = u_0 + \mathrm{vel}_u t + \sum_{n=1}^{n_{\max}} A_n \cos(n\omega t - \phi_n). \quad (7)$$

However, some datasets require secular acceleration as well, giving a *quadratically displaced Fourier series*:

$$u(t) = u_0 + \mathrm{vel}_u t + \frac{\mathrm{acc}_u}{2} t^2 + \sum_{n=1}^{n_{\max}} A_n \cos(n\omega t - \phi_n). \quad (8)$$

Equation 7 or, in certain instances called out below, Eq. 8, is the model we use to describe the motion of a single body point in a single dimension of uv-space, usually with $n_{\max} = 2$ to include the fundamental and first harmonic. Series expansion of relative motion caused by sinusoidally varying flexion shows that these two frequencies should include the majority of the motion of the fish. Because we have 31 body points each requiring two coordinates, a full model of the motion of the fish within its inertial frame requires 62 functions of the form given in Eq. 7 (or Eq. 8).

2.7 Summarizing the harmonic structure of swimming kinematics

To visualize the information in these models we use plots of harmonic structure (see Fig. 8). These plots consist of an array of shapes that indicate the magnitude and phase (if applicable) of the contribution of a particular term in the model (Eqs. 7, 8) at various points along the length of the fish. In these plots, the horizontal dimension represents position along the fish from rostrum on the left to caudal tip on the right. Above the central axis is data on the fit in the lateral direction, below the axial direction. For the secular velocity term, a black square is included for each body point. Sides parallel to the coordinate axes indicate the velocity is in the positive direction for its coordinate, otherwise the square has diagonal sides. A secular acceleration term, when included, is represented by a triangle, which points upward for positive acceleration.

The frequencies used in the model increase as we move outward from the central axis of the plot. The amplitude of the contribution of each frequency is indicated by the area of a disk, while the phase of the contribution is indicated by

the color of the disk, as indicated in the legend accompanying the figure.

These plots include a graphic summarizing the quality of the fit at each point in each component in a row of rectangles at the top and bottom margins of each plot. Each box conveys the R^2 value for the fit at a body point in one dimension. Values of R^2 greater than 0.5 are indicated by filling the box to a level proportional to the excess, beginning at the side closest to the central axis and using black. Values less than 0.5 are indicated by filling the box in red to a level proportional to the deficit, beginning away from the central axis.

3 Results

3.1 Comparing whole body cycle period with tailbeat period

For steady locomotion with large average speed, the visual technique commonly used by biologists to compute a tailbeat period (See Sect. 2.4) gives cycle periods generally comparable to the whole body cycle period. However, when the motion is unsteady and the average speed is small, it is much more difficult to ascertain the fundamental period for the motion. Because the backward swimming trials are generally more unsteady than the forward motion trials, as shown in Fig. 5, and they generally have lower average speeds, as shown in the first graph of Fig. 6, this means that the visual method is unsatisfactory in analyzing these trials in particular. Figure 2 shows that while the tailbeat period computed by an experienced experimenter generally agrees with those computed using the method developed here for the forward trials, there are substantial deviations between the two techniques for the backward trials.

The fact that these deviations show no systematic bias suggests that the differences in these two methods of measurement is not amenable to correction by some fixed adjustment, such as a regression formula. Rather, the statistical technique must be applied to the raw data in order to appropriately estimate the cycle period.

3.2 Unsteadiness index and steady locomotion

The UI allows us to characterize a continuum of body motions (Fig. 3). For the sake of discussion, we categorize all motions with an UI greater than one, when the fish is

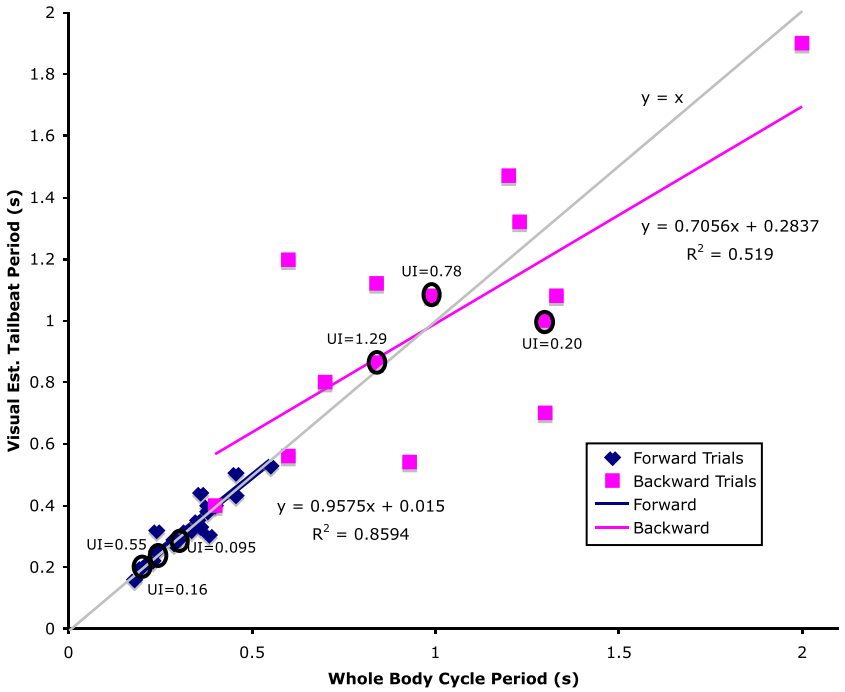

Fig. 2 Tailbeat periods for the 34 trials as found by an experienced experimenter plotted against the whole body cycle periods as computed by the technique described in Sect. 2.4. The plot shows that the two measures of the period of motion generally agree for forward trials, which characteristically have higher speeds and steadier motion. For backward trials, at slower speeds and with more unsteadiness, the measurements differ more substantially. Among backward trials, one notable exception is the only backward trial with cycle period (by either method) less than 0.5 s, where the majority of forward swimming trials lie. This trial also happens to be the fastest of the backward trials, some 40% faster than the next fastest. Although this trial is unsteady (UI = 1.30), the increased velocity seems to make it easier for the experimenter to accurately assess the direction of motion, and therefore the extremes of tail tip motion

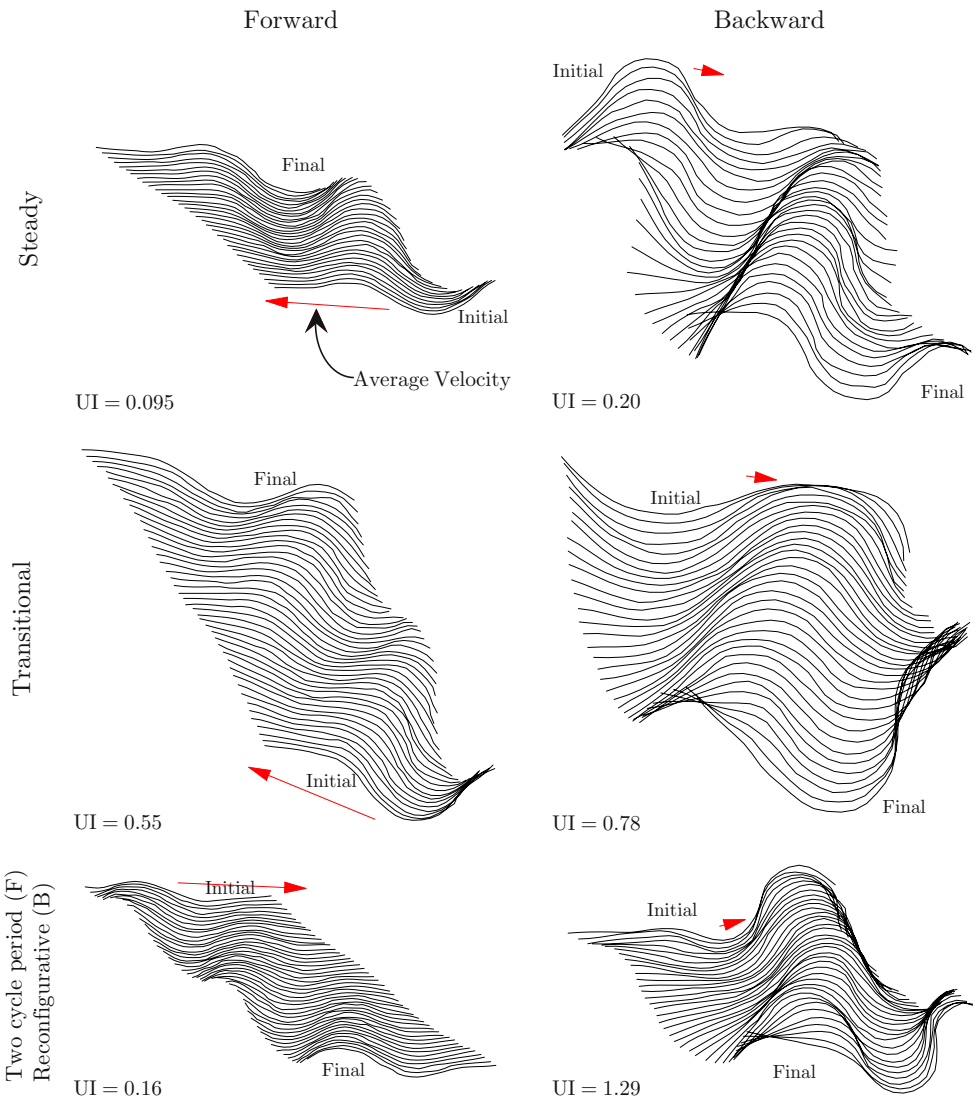

Fig. 3 Behavioral range of forward and backward volitional swimming, as measured and categorized (steady, transitional, or reconfigurative) by unsteadiness index (*UI*). Six examples. Note that *midlines*, normally superimposed, have been displaced laterally to show propagation of curvature and changes in body shape (reconfiguration). The *red arrow*, next to the initial midline in each time series, indicates the average velocity vector for that trial. Reconfigurative swimming occurs only in backward trials (see Fig. 5). The two bottom-most forward swimming trials are the only ones for which two full cycles were captured

using more than half its motion to reconfigure its body, as *reconfigurative* motion. When UI < 0.5 we call the motion *steady*. We denote motion in between reconfigurative and steady as *transitional*. The two steady trials shown as examples are moderately short extensions of a single cycle period, having eight frames (for the forward trial) and six frames (for the backward trial) more than the estimated cycle period (Fig. 3).

Unsteadiness index is sensitive to the number of available frames, since it compares the configurations of the midline in frames separated by a cycle period p (Fig. 4). The steady backward trial (Fig. 3), which has the lowest UI of any backward trial, is one of three that is quantitatively different from the rest, and more like the steady forward trials. Despite this, with 25% fewer frames, it has roughly twice as large a UI as the steady forward trial shown, which, although not the trial with the lowest UI, is still remarkable for the small UI obtained with so many frames. The two cycle forward trial (lower left, Fig. 3), is similarly remarkable for its low UI with 26 frames beyond a cycle period.

The two transitional trials illustrate lack of steadiness in backward swimming, and the importance of considering the number of frames used in the computation of the UI. The forward transitional trial is one of only two trials that contains more than two full cycle periods, having 23 frames past a cycle of 20 frames. This by itself is not enough to account for the higher UI, as the third forward trial shows (Fig. 4), but its UI is not far from the value predicted by forward trials as a whole. Compared to the other two forward trials, the transitional trial includes a reconfigurative component with motion that is otherwise fairly steady (Fig. 3).

Comparison of the two transitional trials (Fig. 3) shows the backward trial's motion is much less steady, despite being the steadiest of all the backward trials except the

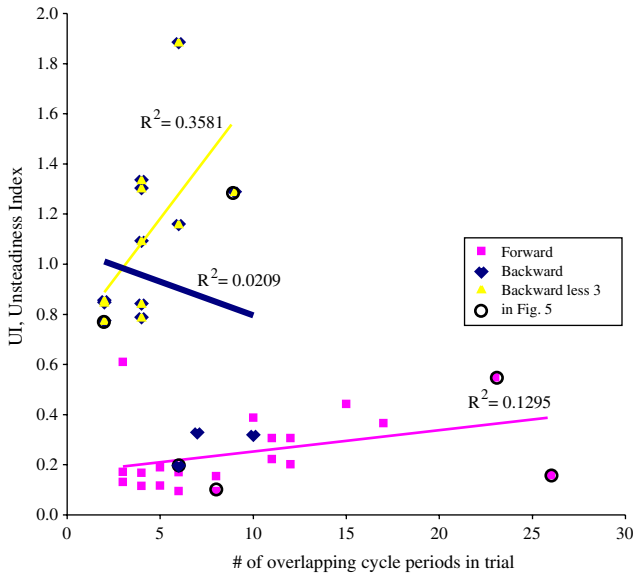

Fig. 4 The number of frames analyzed alters UI. The association for forward and most backward trials is clearly different, however, there are three backward trials (shown by *blue markers*) that follow the forward trial association. When they are included with all backward trials their effect on R is substantial, driving it to essentially 0, actually making it slightly negative. When they are excluded, however, we see that the R for both sets of trials are appreciably positive

three outliers. This trial includes only two frames more than a cycle period, and this shorter relative length is typical of backward trials (Fig. 4). This transitional trial has more in common with the third, reconfigurative, backward trial; both show substantial reconfiguration with very little displacement, as witnessed by their short average velocity vectors (shown in red, Fig. 3).

As shown in Fig. 4, the association between UI and number of frames analyzed is different for forward and backward motion. For forward trials, the association is fairly strong and linear, while for backward trials it is quite weak. In addition, the two regression lines have different slopes and more importantly different intercepts; neither of them zero. This precludes time averaging UI to obtain a parameter independent of the number of frames, as it would artificially penalize shorter trials.

While this time dependence of UI is a weakness, it displays a basic feature of this technique. Long trials, measured in terms of the cycle period rather than seconds, have more opportunity to be unsteady, and by and large are more unsteady.

3.2.1 *Steadiness and direction of locomotion*

When the UI for all 34 trials are compared (Fig. 5), we find clear separation of forward and backward swimming. Backward trials demonstrate more unsteadiness, and more variability in unsteadiness, in spite of the fact that they show less variablility in p and $\hat{\mathbf{v}}_{ave}$ than forward trials (Fig. 6). The backward and forward trials show no appreciable association between UI and either cycle period or swimming speed. If we disregard the high UI outlier trial, there is a *negative* association between UI and p (r = –0.744), suggesting that slower tail undulations and steadier motion are correlated, *only in backward swimming*.

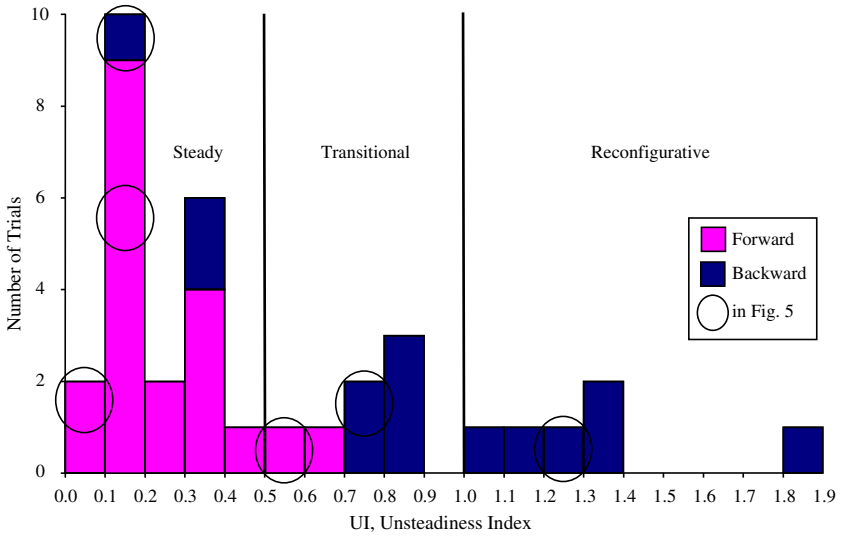

Fig. 5 Unsteadiness indexs for forward and backward swimming occupy separate modes in a biomodal distribution. The forward swimming trials form the preponderance of the primary mode within the steady category (0.1 < UI < 0.4), while the secondary mode (0.7 < UI < 1.4) is comprised entirely of backward transitional or reconfiguring trials. The largest UI is an outlier even among backward trials, which demonstrate more than twice the variability in UI of the forward trials. ($s_{backward}$ = 0.46, and even ignoring the outlier the standard deviation of the other 13 backward trials is 0.385, while $s_{forward}$ = 0.15)

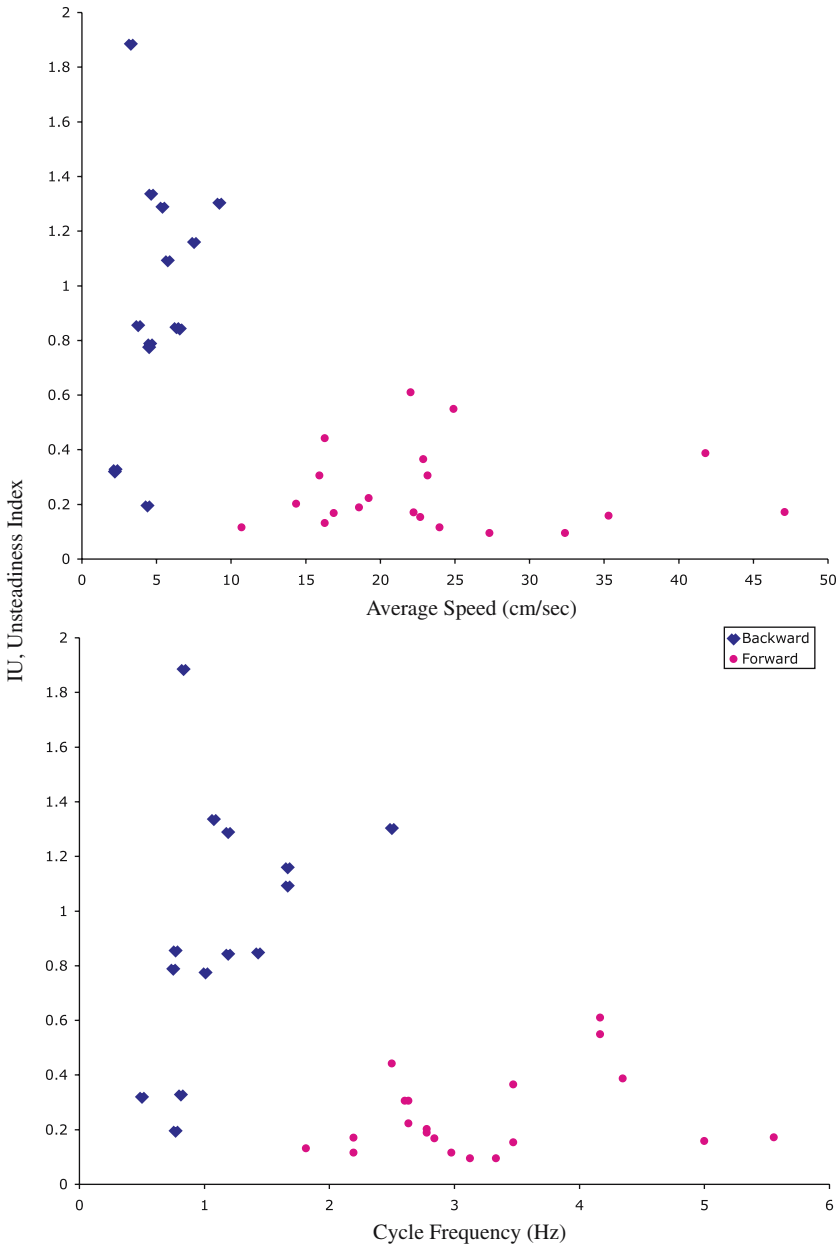

Fig. 6 When correlated with swimming speed and WBCF, the values for UI of forward and backward swimming form non-overlapping clusters. Compared to forward swimming, backward swimming is characterized by UIs with a greater range, slower speeds, and, with one exception, slower cycle frequencies

3.2.2 Reconfiguration errors and steady swimming

Differences between steady and unsteady swimming are also detected and characterized by the REs (Fig. 7). The pattern in the REs demonstrates that lamprey in the backward swimming trials (on the right) are engaged in more reconfiguration than during forward swimming. The tight cluster of the REs for forward trials is partly attributable to the greater speed, since these errors are all relative to average speed. Even allowing for this, there is substantially more reconfiguration, especially in the two least steady backward trials shown. Compare these with the transitional forward trial, where most errors are relatively tightly clumped, but the fish gradually reconfigured by sweeping its tail downward over the end of the two cycle trial.

We can see this because generally REs for later cycle period windows are larger than those for earlier windows, and, in this case, a comparison of the initial frames with the final frames (see Fig. 3), shows that the tail's upstroke is less extreme at the end of the trial. Compare this with the REs of the transitional backward trial (see Fig. 7). There are many fewer errors computed in this trial, only two frame's worth, compared with 23 for the corresponding forward trial, but the backward trial's reconfiguration errors are larger, in both absolute and relative (to speed) terms. The plot shows that, relative to the body as a whole,

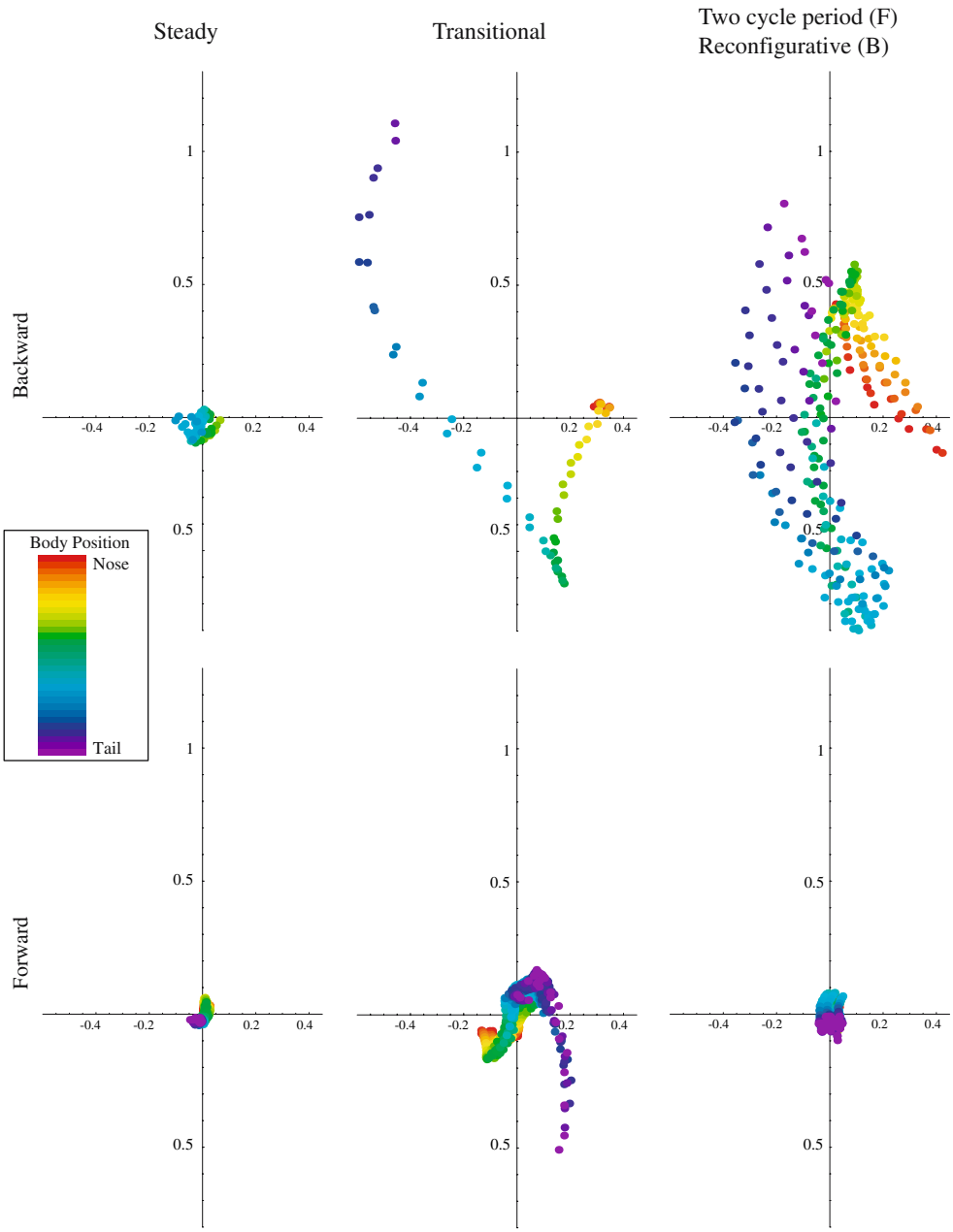

Fig. 7 Reconfiguration errors (*REs*) for the representative trials illustrated in Fig. 3 are relative errors in estimates of the average speed as defined in Eq. 4. The change in scale amongst the plots is the most important basis for comparison. These plots are transposed from the positions of the corresponding plots in Fig. 3; rotate this figure 90° clockwise to place these plots in the corresponding positions

the caudal region is reconfiguring up and to the the left, over just a little more than one cycle. Looking at the motion of the backward transitional trial (Fig. 3), we can see that this is the what has actually happened; the fish arches its leading edge (tail) up and leftward. While reconfiguration occurs in forward steady swimming, it tends to be both smaller in magnitude and more gradual in occurance than during backward swimming.

Comparing the backward transitional and reconfigurative trials, we see the latter group has no errors as large as the largest in the former; instead it has many more errors, nine frame's worth. Thus, while the reconfiguration across any individual cycle period is less for the latter, because it is longer (measured in cycle periods), it allows for more reconfiguration to occur. This is apparent from the motion (Fig. 3), where the reconfiguration from the initial to the final frame in the reconfigurative trial is more extreme than in the transitional trial. This qualitative observation is suspect because the initial and final frames of a trial are not typically at the same phase of a cycle period, and so the periodic component may appear to be reconfigurative. This idea can be made more rigorous by filtering out the periodic components of the motion as described in Sect. 3.3.2. However, the UI allows us to state that the reconfigurative trial is 65% more unsteady than the transitional trial.

3.3 Harmonic structure of undulatory swimming

The entire dataset for each of the 34 trials was analyzed. The resulting fitting functions have the form of Eq. 7 with $n_{max} = 2$. The fitting functions can be used to compute many kinematic parameters generally used to quantify motion of a swimming fish. These include not just mean velocity and tailbeat frequency, whose generalizations, $\hat{\mathbf{v}}_{ave}$ and p, have already been discussed extensively. The fitting functions also allow estimations of head-tip and tail-tip amplitude, propulsive wavelength, wavespeed, stridelength, lateral curvature, relative power, Reynolds number, Strouhal number and Froude efficiency in ways that give weight to all the data collected, rather than depending upon the measurement of a small number of points to characterize the entire motion. As an example of this, we examine these trials for the presence of an accelerating wave of curvature in Sect. 2.3 below. First, we examine the harmonic structure of the six representative trials of Fig. 3 by means of harmonic structure plots, as described in Sect. 2.7.

3.3.1 Visualizing harmonic structure

Our kinematic analysis of the whole body is summarized by harmonic structure plots (Fig. 8). Each plot displays the information contained in 62 linearly displaced Fourier series that describe the motion of one of the trials.

The plot of the forward steady trial shows basic features of steady locomotion. The secular velocity terms in both the lateral and axial dimensions are small, while the lateral fundamental frequency is large, and grows approaching the trailing edge (the caudal tip in this trial). The periodic contribution in the axial direction is small and the fundamental component has roughly constant phase. The axial first harmonic component grows in amplitude with the amplitude of the fundamental lateral component. The phase of the lateral fundamental shows that the body has roughly one and a quarter waves on it. Also, the phase decreases steadily as we move posteriorly, indicating a wave traveling down the body. Examining R^2, we see that the fit in the lateral direction is excellent, with over 90% of the motion accounted for by this model at every point on the body. The fit in the axial direction is worse, since the data have been transformed to remove the displacement due to the average velocity of the fish. Thus for a steady trial like this, there is very little axial motion left, and the error is relatively larger than in the lateral dimension.

The steady backward trial has some of the features just delineated, but also notable differences. Most obvious is more uniform amplitude of lateral fundamental components of the model. Although the smallest amplitude occurs at the leading edge (the caudal tip), that amplitude is nearer to maximum than in the forward trial. (Sizes are scaled relative to the maximum fundamental lateral component, thus relative sizes within a plot are meaningful, but comparison across trials is inappropriate.) Further, amplitudes increase moving anteriorly until roughly 30% of a fish-length from the rostral tip. Amplitudes decrease to roughly the 10% mark, and then increase to the rostral tip. Presence of a second local maximum amplitude point, as well as more nearly uniform amplitude along the whole fish, are common characteristics of backward swimming trials not shared by forward swimmers. Note that the phases of lateral fundamental components indicate both a longer wavelength (just over one wave on the body), and that the wave travels forward in this trial, since the phase decreases moving anteriorly.

The lateral fit for this trial is slightly worse than in the steady forward trial, as the REs suggest (see Fig. 7); however, the fit in the axial direction accounts for substantially more of the motion contained in the data. This is because of larger axial components; this trial has more axial motion left when displacement due to composite average velocity is accounted for. The high R^2's show that the reconfiguration taking place in this trial is occurring with roughly constant velocity at each body point, since the model, including secular velocity, yields an excellent fit to the data.

Looking at the backward transitional trial, it is clear that the model's fit to this trial is even better than either of the two trials considered to this point. The ability of a model for steady locomotion to fit so well to data that is not steady lies in the inclusion of secular velocity. Note the increase in magnitude of these components compared to the steady trials. The squares (or diamonds) symbolizing velocity are scaled so that their area is comparable to the area of a disk for a fundamental frequency component that has the same average speed over a cycle period. So, we can see that at the caudal tip, the secular velocity term is causing more displacement than the periodic motion, because it has larger average speed. If the secular dominates the periodic over the entire length of the fish, then motion would be reconfigurative. As it is, this plot agrees with its classification as transitional.

3.3.2 Excising the periodic component of motion

To remove the periodic component of the fitting functions in a model, leaving the "average" position of the fish at any moment, we set the coefficients of the cosine terms in either of Eq. 7 or 8 to zero, leaving only the secular terms. This average position can be used to identify reconfiguration of the fish independent of periodic motion.

Consider the comparison offered by Fig. 9 of the two bottom-most trials in Fig. 3. Displaying initial and final frames of the two trials with both the actual and average

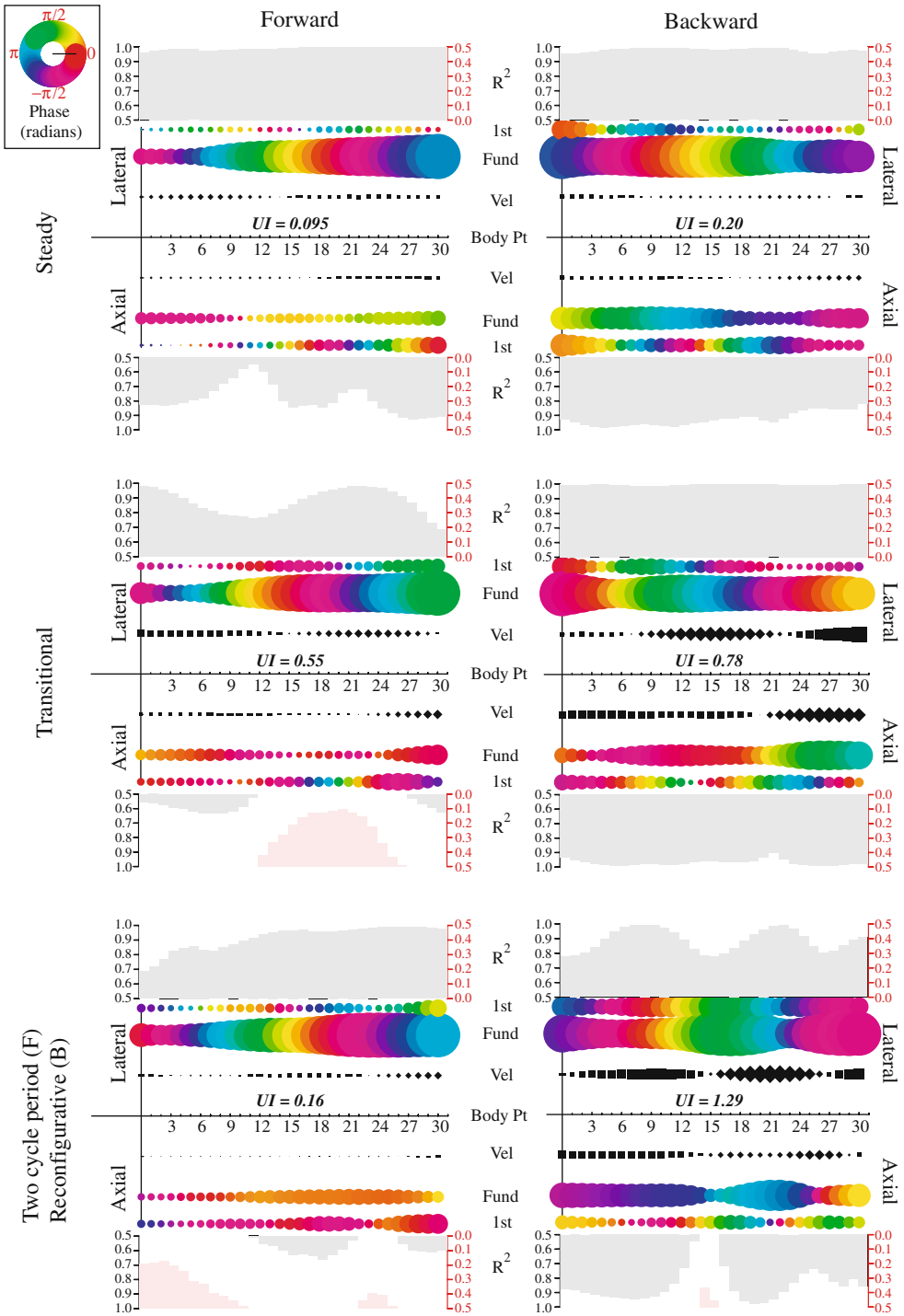

Fig. 8 Harmonic structure for the each of the six swimming trials shown in Fig. 3. Structure of the lateral and axial motion of each point is shown above and below, respectively, the horizontal axis. Harmonic structure measured as the amplitude (area of point) and phase (color of point) of the fundamental and first harmonic frequency of each point relative to the others in that trial and direction (lateral vs. axial). Secular velocities for each point in each direction is also shown. Accuracy of the harmonic model in capturing the motion of one point in one dimension indicated by the R^2 values, which are read from the scale on the left when *black*, and the scale of the right when *red*. Further description of these graphics is given in Sect. 2.7, and they are interpreted in Sect. 3.3.1

positions requires reintroducing the composite average velocity to the model (It was removed as described in Sect. 2.6.), as well as excising the periodic terms. The forward trial has very little reconfiguration, just a slight downward motion of the tail, and a compensating upward motion in the precaudal region. Over the 1.26 cycle periods of the unsteady trial, the translation in the axial direction of the fish is dwarfed by the lateral leftward (in the fish's frame of reference) motion of the midsection and corresponding rightward motion of its extremities. These results are consonant with the REs for these trials (Fig. 7), but they derive from Fourier analysis, rather than from comparison of frames separated by a cycle period. Examining Fig. 7, the REs for the forward trial shows REs of neighboring body points are necessarily grouped together, and the errors tightly clustered about the origin. The density

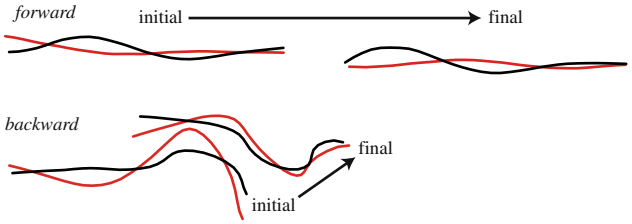

Fig. 9 Forward swimming is primarily translational while backward swimming combines translation and reconfiguration. The *black curves* represent the actual body midlines of the lampreys, while the *red curves* represent "average" positions at the same instants, as defined in Sect. 3.3.2. These average positions average out periodic undulatory motion, leaving the net positions that change aperiodically. Data from trials shown in the bottom row of Fig. 3; UI = 0.16 (*top*) and 1.29 (*bottom*). The differences in the positions of the initial and final *black curves* in the figure reflect the actual movement of the fish (as contrasted with Fig. 3). The differences in the positions of the initial and final *red curves* show the aperiodic change in the average position and configuration of the fish. Specifically, for the backward trial, the differences in the shapes of the initial and final *red curves* demonstrate the prediction of the REs shown in Fig. 7 that the fish undergoes a major displacement in the form of a U-shaped reconfiguration that dominates the translation of the fish in this trial. This deformation is not the result of periodic undulation, as this figure demonstrates. In comparison, the change in the initial and final averaged positions for the forward trial show that this trial is dominated by translation, with relatively little reconfiguration. This agrees with the REs for this trial, shown in Fig. 7

decreases roughly uniformly regardless of the direction of departure from the origin, but errors with negative y-component are for the caudal region, while those for pre-caudal to mid-fish points have positive y. The average positions in Fig. 9 confirm that reconfiguration in the raw data is not simply due to a change of phase, but rather to secular reconfiguration of the fish.

3.3.3 Number of waves on the body

By summing phase differences from one body point to the next for the fundamental frequency in the lateral direction, it is possible to compute the total phase difference from the tail to the end of the fish; dividing by 2π yields the number of traveling waves computed in a fashion that takes into account all the available data, and therefore more accurate than a visual estimate based on a single frame (Long and Nipper 1996). Based on this data we can assert that there is no important association between UI and waves on the body, but that backward swimmers have roughly one quarter fewer waves on the body than forward swimmers, since the mean for the forward trials is 1.46 with standard deviation $s_{\text{forward}} = 0.15$, while the backward trial mean is 1.20 with $s_{\text{backward}} = 0.21$. Lamprey use smaller wavelengths proportional to body size for forward swimming, as compared to backward swimming with $P = 0.0003$, $t = 3.98$, $df = 22.02$.

Linear regression of the phases of the fundamental frequency in the lateral dimension is another means to estimate the number of waves on the body; it also permits identification of acceleration of the traveling wave. The quotient $2\pi/m$ is the best estimate for the wavelength λ, assuming a traveling wave of the form $A(x)\cos(\omega t - 2\pi\, x/\lambda - \varphi)$ describes the overall motion. Here, x is distance from the rostral tip, and the other quantities are as described in Sect. 2.6. The results for five of the six trials shown in Fig. 3 are shown in Fig. 10. The wavelength is substantially constant along the length of the lamprey in all these trials. Beyond this, the plot shows a pattern in those small deviations from constancy: near the leading edge, phase is consistently underestimated by the regression line, indicating a longer wavelength in this region. Downstream there is a portion of the body, between roughly 1/6, and 1/3 fish-length from the leading edge, where phase changes are greater than predicted by the regression line, indicating a region where the wavelength is shorter. Thereafter, phase changes in the forward trials settle close to the line. In the backward trials, deviations are more pronounced, and the pattern on the more anterior portion of the fish is less clear. The steady trial seems more like the forward trials, while the two less steady trials show deviations in wavelength along the entire length of the fish.

3.3.4 The speed and amplitude of undulatory waves

In all forward swimming trials except the least steady, amplitude of the lateral wave of deflection is decreasing posteriorly at the rostral tip. While the point where minimum amplitude occurs varies from trial to trial, it is generally 10% of body length from the rostral tip. Posterior of this point, the amplitude increases roughly exponentially, but often with a stairstep appearance (Fig. 11). The three forward trials all show this profile, although the steadiest trial appears to have a change in the rate of exponential growth at a point 1/3 fish-length from the rostrum. At this point more rapid exponential growth seems to change to growth that is still exponential with a lower rate. The other two trials display stairsteps indicating a roughly constant rate of growth but with fluctuations along the length of the fish. Using the analysis of Cheng and Blickhan (1993), this suggests comparable fluctuations in the speed of the wave of curvature.

The amplitude profile of lateral deflection for backward swimmers is remarkably different. In all three trials (see Fig. 11), average amplitude is much larger, and amplitude is increasing at the leading edge, moving downstream. The amplitude reaches a peak just downstream of the leading edge and then drops to a minimum less than 1/3 fish-length from the leading edge. From there it rises to a second local maximum somewhere in the middle third, before falling to

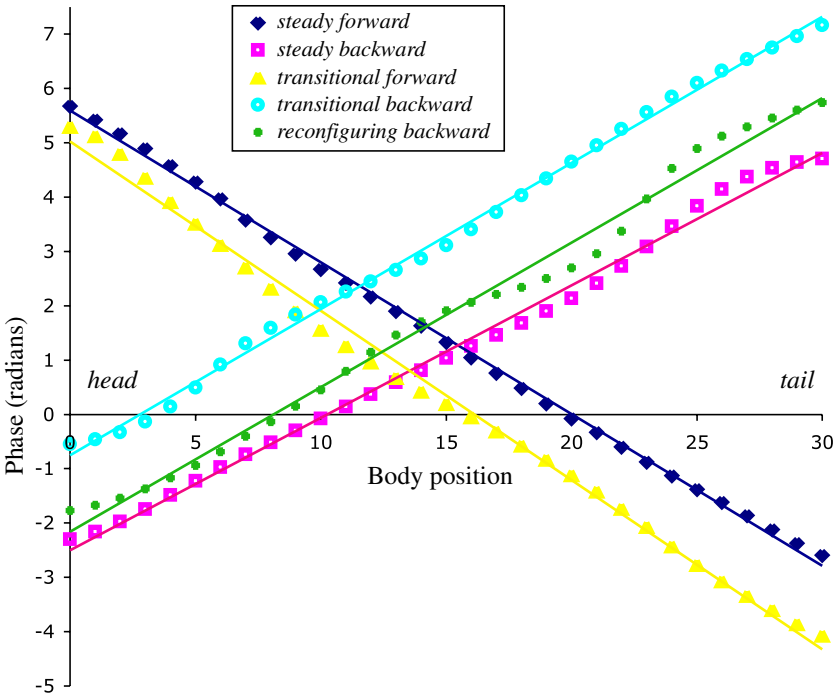

Fig. 10 Phase of the fundamental frequency in the lateral direction differs only in sign between forward and backward swimming. Data for five of the representative trials shown in Fig. 3. (The final forward trial is omitted for clarity.) In addition, the regression line in each case represents a fixed propulsive wavelength on the fish's body; each fit has a $R^2 > 0.99$

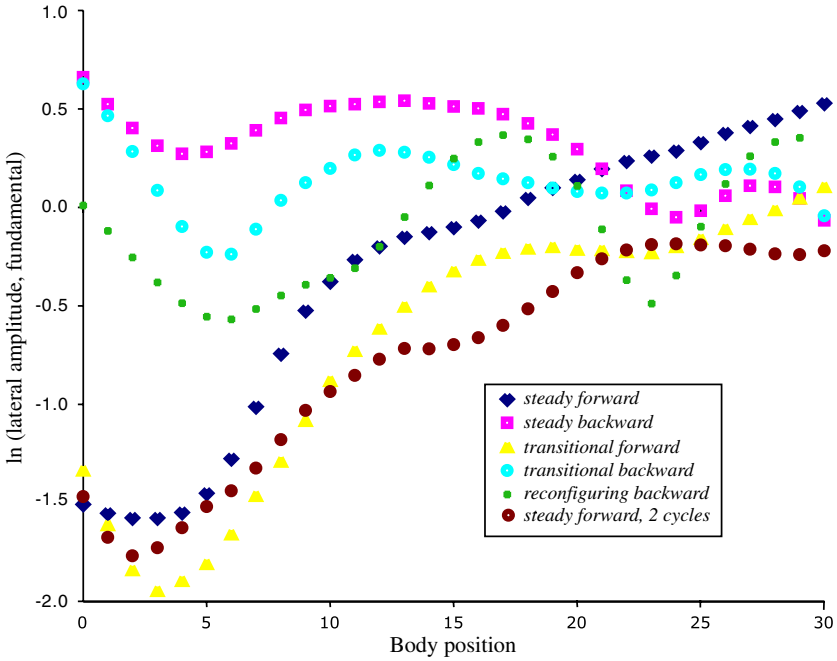

Fig. 11 Lateral amplitude profile of the fundamental frequency differs between forward and backward swimming. Data for the six representative trials shown in Fig. 3. Compare the increase in amplitude with body position for forward swimming with the relatively constant amplitudes for backward swimming

a local minimum 1/6 of a body length from the trailing edge. From that minimum, amplitude rises exponentially to the rostrum. Fluctuations near the leading edge are less pronounced in the two steadier backward trials, and the local minimum near the trailing edge is more marked in the two less steady trails. Despite these deviations, more remarkable are similarities shared by these trials, and their difference from forward swimming profiles.

3.4 Secular acceleration as a deviation from steadiness

Our technique allows us to identify secular acceleration in motion that superficially appears to be steady swimming. The utility of this technique is apparent in comparing the models of the two less steady forward trials (Fig. 8) with models incorporating a secular acceleration term (Eq. 8, see top row of Fig. 12). Inclusion of the acceleration term

offers remarkable improvement, especially for the less steady of the two trials. Perhaps more remarkable is the comparison of the fits incorporating acceleration with fits that add higher harmonics to the base model (see bottom row of Fig. 12). Despite using seven additional degrees of freedom at every body point, the higher harmonic models have lower R^2 values than the secular acceleration models, showing that secular acceleration is more important than higher harmonics in describing the motion observed in these trials.

4 Discussion

Here we present a method that analyzes, via a mathematical decomposition, whole-body kinematics of an important category of fish swimming behaviors—single propulsive cycles of translation with superimposed elements of harmonic and secular motion. After determination of the body's propulsive cycle and frequency, this method uses harmonic analysis and statistics to identify and characterize different behaviors. For example, forward and backward swimming motions in lamprey are similar in terms of the pattern of phase lag of the fundamental harmonic, but they differ in their unsteadiness. This method also makes possible analysis of kinematic changes in behavior of a single individual, a capability that, while not used in this study, should interest researchers needing detailed kinematic inputs to open-loop models or accurate tests of validation of outputs of closed-loop models.

Using this method, we found three important general conclusions about swimming lamprey: (1) they can superimpose periodic and secular components of body motion, (2) they can modulate the relative magnitudes and axial patterns of the superimposed periodic and secular components, and (3) they can change shape. We are left with a novel hypothesis—the seemingly simple act of steady swimming is a maneuver requiring active minimization of secular motion and body reconfiguration.

4.1 The whole-body kinematics of forward and backward swimming

Prior to our analysis, we had two different expectations: (1) that backward swimming in lamprey was simply forward swimming with reversed direction of body flexure propagation (Grillner 1996) and (2) that backward swimming in lamprey, based on that in eel, would involve much larger lateral displacements over more of the body than forward swimming (D'Aout and Aerts 1999). We found support for both. Even though lateral amplitudes of the fundamental frequency fits the pattern seen in eels (Fig. 11), the phase lag pattern of the lateral amplitudes of the fundamental frequency for backward swimming is equal and opposite to that of forward swimming (Fig. 10). Surprisingly, both amplitude and phase lag results for forward or backward swimming are independent of unsteadiness. In other words, the kinematic behavior of the fundamental harmonic motion of the body—arguably the basis of steady locomotion—can be analyzed and compared independently from secular components of motion, velocity and acceleration. This also suggests that neural mechanisms controlling steady locomotion can have superimposed upon them other neural mechanisms that control secular motions, including body reconfiguration. While local central pattern generators control, with feedback from stretch receptors (Sigvardt 1989), the steady kinematics, work on startle responses (Ritter et al. 2001) suggests a parallel and superimposable neural system mediated by the reticulospinal network.

Further, compared to forward swimming, backward swimming has fundamentally different kinematics: it is more reconfigurative, i.e., less steady. Backward swimming frequently also includes larger deviations in wavelength along the fish, although this is not present in the steadiest trials. This follows from a different physiology of motion: in backward swimming, points along the fish tend to follow the trajectory of points nearer the leading edge. Some of the differences between forward and backward swimming are likely to be caused by lamprey's head-retraction startle response and its associated body reconfiguration (Currie and Carlsen 1985, 1987). The startle mechanism may explain correlation between rapid cycle frequencies and high UIs in backward swimming of juvenille lampreys. Under the conditions examined here, we also see that behavioral flexibility varies with swimming direction. Forward swimming occurs over a greater range of swimming speeds and cycle frequencies than backward swimming.

4.2 Unsteady swimming and changing body shape

According to our definition, steady swimming contains unsteady elements and unsteady swimming contains steady elements. When we incorporate secular acceleration to model body kinematics, forward motion trials show rapid, small reconfigurations achieved by independent acceleration of different segments along the length of the body in the course of one or two cycle periods. In contrast, reconfiguration in backward trials, while also present, tends to be slower and steadier, and can be modeled with secular velocity alone. The ability to accurately model backward reconfigurations without secular acceleration indicates that they are achieved by steady differences in velocity of segments of the fish. The two conclusions are unexpected: (1) lamprey change shape, they reconfigure, as the swim

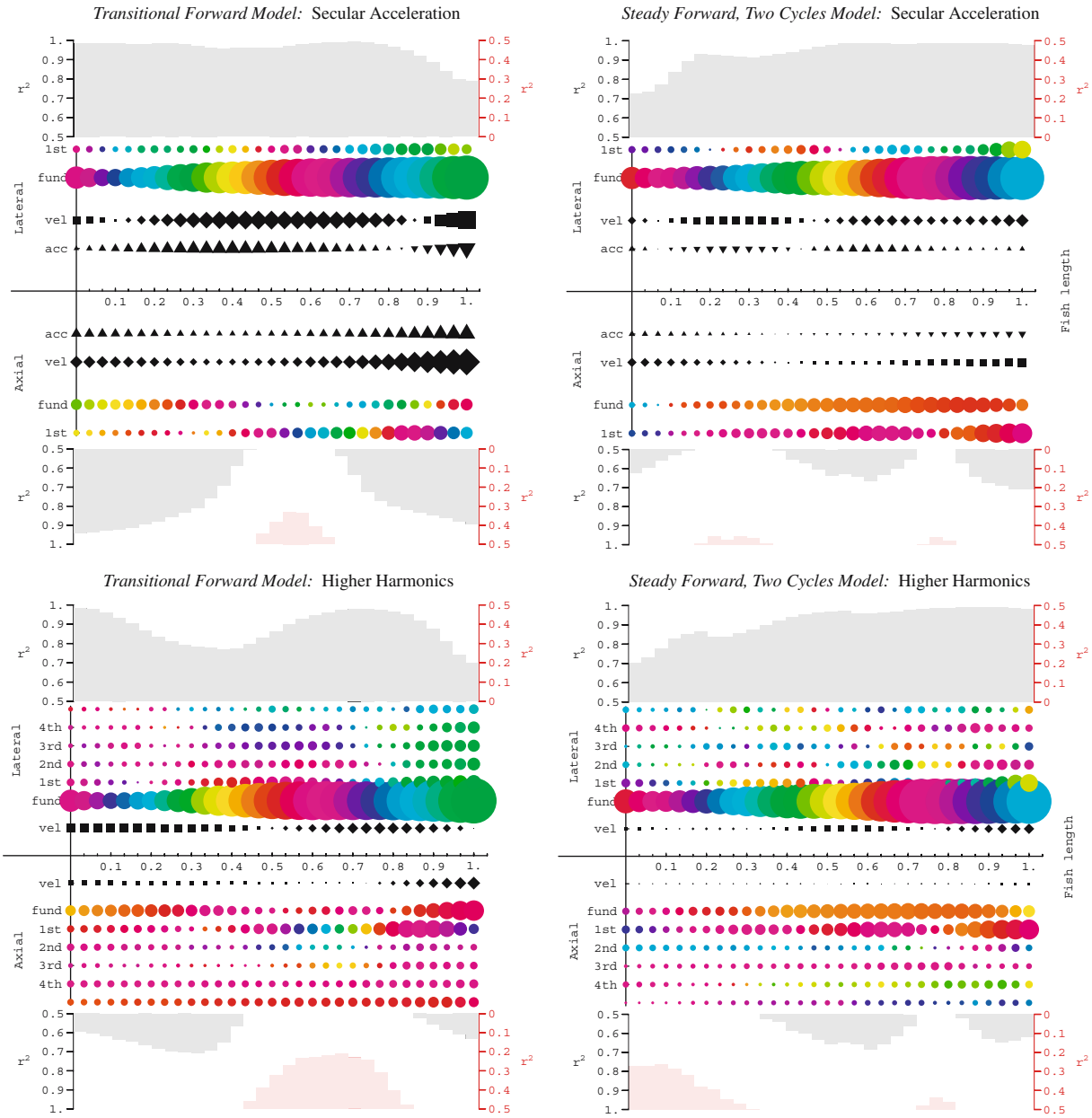

Fig. 12 Models with secular acceleration give a superior fit compared to those with just higher harmonics and no secular acceleration. Two examples are given (from Fig. 2): the transitional forward swimming and the steady two cycle forward swimming trial. Secular acceleration is included in models of the *top row* and is indicated by *triangles*. In spite of the much larger number of parameters included in the models with higher harmonics (seven more at each body point; see *bottom row*), in both cases models with secular acceleration give better fits for both axial and lateral dimensions. See Sect. 2.7 for a more detailed description, and Sect. 3.4 for a more detailed interpretation of these plots

and (2) they change shape in different ways depending on the direction of swimming.

While we have not analyzed steady swimming within the experimental paradigm of flume studies, our analysis shows that motion classified as steady in a still-water tank shows considerable variation, typically more than the 5% threshold set by Jayne and Lauder (1995). REs for the four trials with the smallest UIs all display variation greater than 5%, and for two of them, including the trial with the best UI in the dataset, the rostral tip displays errors greater than 5%. However, only the trial with the worst UI of the four has REs larger than 10%, and only near the caudal tip. Note that these REs include two dimensions, while Jayne and Lauder considered only the axial dimension.

4.3 Growth of displacement amplitude and wavespeed of curvature

Many authors have noticed that undulatory locomotion must display accelerating waves of curvature (e.g., Hess and Videler 1984; Katz and Shadwick 1998). An equivalent expression to a constant velocity wave of curvature is that the amplitude of deflection increases exponentially along the body (Cheng and Blickhan 1993). Thus a simple way to test for accelerating curvature is via amplitudes of fundamental frequency contributions to lateral motion. If logarithms of these amplitudes are concave up, indicating that the growth in amplitude is super-exponential, then the wave of curvature is accelerating. Conversely, concave down logarithms indicate decelerating curvature. Using this criterion, none of the 34 trials showed consistently accelerating waves of curvature. Instead amplitudes seem to fluctuate from concave up to concave down, indicating that curvature is changing velocity as it propagates.

4.4 Extension of the technique

The analytical technique we apply to swimming lamprey can be extended to other maneuvers. Only Eq. 1, which insists on only periodic acceleration which averages to zero, constrains the model to steady swimming. By incorporating secular acceleration constant across the extent of the fish, the model can analyze (1) linear accelerations like that associated with S-type fast starts and (2) rotational accelerations involved in turns. Moreover, if we allow secular acceleration to vary along the fish, the model applies to more intricate maneuvers, like C-type fast starts. These extensions require careful limitations on secular terms in order to maintain the model's simple form.

Acknowledgments The authors gratefully acknowledge grant support from the US Office of Naval Research, #N00014097-1-0292 and from the US National Science Foundation, #DBI-0442269 and #BCS-0320764. We thank Eamon Twohig for his work on the harmonic analysis.

References

Arena P, Fortuna L, Frasca M, Vagliasindi G (2006) A wave-based cnn generator for the control and actuation of a lamprey-like robot. Int J Bifurcat Chaos 16(1):39–46

Bierman HS, Schriefer JE, Zottoli SJ, Hale ME (2004) The effects of head and tail stimulation on the withdrawal startle response of the rope fish (*Erpetoichthys calabaricus*). J Exp Biol 207(22):3985–3997

Blickhan R, Cheng JY (1994) Energy storage by elastic mechanisms in the tail of large swimmers a re-evaluation. J Exp Biol 168:315–321

Bowtell G, Williams TL (1993) Anguilliform body dynamics: a continuous model for the interaction between muscle activation and body curvature. J Math Biol 32:83–92

Brockwell PJ, Davis RA (1996) Introduction to time series and forecasting. Springer texts in statistics. Springer, New York

Carling JC, Williams TL, Bowtell G (1998) Self-propelled anguilliform swimming: simultaneous solution of the two-dimensional navier-stokes equations and newton's laws of motion. J Exp Biol 201(23):3143–3166

Castro-Santos T (2005) Optimal swim speeds for traversing velocity barriers: an analysis of volitional high-speed swimming behavior of migratory fishes. J Exp Biol 208:421–432

Chatfield C (2004) The analysis of time series: an introduction, 6th edn. In: Texts in statistical science. Chapman & Hall/CRC, Boca Raton

Cheng JY, Blickhan R (1993) Bending moment distribution along swimming fish. J Theor Biol 168:337–348

Cheng JY, Pedley T, Altringham J (1998) A continuous dynamic beam model for swimming fish. Phil Trans R Soc Lond B 353:1–17

Crespi A, Ijspeert AJ (2006) Amphibot ii: an amphibious snake robot that crawls and swims using a central pattern generator. In: Proceedings of the 9th international conference on climbing and walking robots (CLAWAR 2006), pp 19–27

Currie SN, Carlsen RC (1985) A rapid startle response in larval lamprey. Brain Res 358:367–371

Currie SN, Carlsen RC (1987) Functional significance and neural basis of larval lamprey startle behavior. J Exp Biol 133:121–135

Dabiri JO (2005) On the estimation of swimming and flying forces from wake measurements. J Exp Biol 207(7):3519

Daniel TL, Coombes SA (2002) Flexible wings and fins: bending by inertial or fluid-dynamic forces? Integr Comp Biol 42:1044–1049

Daniel TL, Tu MS (1999) Animal movement, mechanical tuning and coupled systems. J Exp Biol 202:3415–3412

D'Aout K, Aerts P (1999) A kinematic comparison of forward and backward swimming in the eel *Anguilla anguilla*. J Exp Biol 202(11):1511

Ekeberg O (1993) A combined neuronal and mechanical model of fish swimming. Biol Cybern 1993:363–374

Grillner S (1996) Neural networks for vertebrate locomotion. Sci Am 274(1):64–69

Grillner S, Deliagina T, Ekeberg O, El Manira A, HIll RH, Lansner A, Orlovsky GN, Wallen P (1995) Neural networks that co-ordinate locomotion and body orientation in lamprey. Trends Neurosci 18(6):270–279

Guan L, Kiemel T, Cohen A (2001) mpact of movement and movement-related feedback on the lamprey central pattern generator for locomotion. J Exp Biol 204:2361–2370

Hess F, Videler J (1984) Fast continuous swimming of saithe (*Pollachius virens*): a dynamic analysis of bending moments and muscle power. J Exp Biol 109:229–251

Ijspeert AJ (2001) A connectionist central pattern generator for the aquatic and terrestrical gaits of a simulated salamander. Biol Cybern 85(5):331–348

Ijspeert AJ, Kodjabachian J (1999) Evolution and development of a central pattern generator for the swimming of a lamprey. Artif Life 5(3):247–269

Ijspeert AJ, Hallam J, Willshaw D (1999) Evolving swimming controllers for a simulated lamprey with inspiration from neurobiology. Adapt Behav 7(2):151–172

Islam SS, Zelenin PV, Orlovsky GN, Grillner S, Deliagina TG (2006) Pattern of motor coordination underlying backward swimming in the lamprey. J Neurophysiol 96(1):451–460

Jayne B, Lauder G (1993) Red and white muscle activity and kinematics of the escape response of the bluegill sunfish during swimming. J Comp Physiol A 173:495–508

Jayne B, Lauder G (1995) Speed effects on midline kinematics during steady undulatory swimming of largemouth bass, *Micropterus salmoides*. J Exp Biol 198:585–602

Katz SL, Shadwick RE (1998) Curvature of swimming fish midlines as an index of muscle strain suggests swimming muscle produces net positive work. J Theor Biol 193:243–256

Lachat D, Crespi A, Ijspeert AJ (2006) Boxybot: a swimming and crawling fish robot controlled by a central pattern generator. In: Proceedings of the first IEEE / RAS-EMBS international conference on biomedical robotics and biomechatronics (BioRob 2006)

Lighthill M (1975) Mathematical Biofluiddynamics. Res. Conf. Nat. Sci. Found., 1973, Soc. Ind. Appl. Math. (SIAM), New York

Liu H, Wassersug R, Kawachi K (1996) A computational fluid dynamics study of tadpole swimming. J Exp Biol 199:1245–1260

Long JH Jr (1995) Morphology, mechanics, and locomotion: the relation between the notochord and swimming motions in sturgeon. Environ Biol Fish 44:199–211

Long JH Jr, Nipper KS (1996) The importance of body stiffness in undulatory propulsion. Am Zool 36(6):678–693

Long JH Jr, Root RG, Watts P (2002) Is an undulating fish an oscillating wing? Integr Comp Biol 42(6):1268A

Müller UK, van Leeuwen JL (2004) Swimming of larval zebrafish: ontogeny of body waves and implications for locomotory development. J Exp Biol 207:853–868

Or H, Hallam J, Willshaw D, Ijspeert AJ (2002) Evolution of efficient swimming controllers for a simulated lamprey. In: From animals to animats: Proceedings of the 7th international conference on the simulation of adaptive behavior (SAB2002)

Ritter DA, Bhatt DH, Fetcho JR (2001) In vivo imaging of zebrafish reveals differences in the spinal networks for escape and swimming movements. J Neurosci 21(22):8956–8965

Sigvardt KA (1989) Spinal mechanisms in the control of lamprey swimming. Am Zoo 29:19–35

Taylor GK, Nudds RL, Thomas ALR (2003) Flying and swimming animals cruise at a Strouhal number tuned for high power efficiency. Nature 425:707–711

Tolstov GP (1962) Fourier series. Prentice-Hall, Englewood Cliffs (trans. by Richard A. Silverman)

Triantafyllou GS, Triantafyllou MS, Grosenbaugh MA (1993) Optimal thrust development in oscillating foils with application to fish propulsion. J Fluid Struct 7:205–224

Tytell ED (2004a) The hydrodynamics of eel swimming. ii. Effect of swimming speed. J Exp Biol 207:3265–3279

Tytell ED (2004b) Kinematics and hydrodynamics of linear acceleration in eels, *Anguilla rostrata*. Proc Roy Soc B 271:2535–2541

Ward AB, Azizi E (2001) Hydrodynamics and energetics of fish propulsion. Am Zoo 41:1620A

Webb PW (1975) Hydrodynamics and energetics of fish propulsion. Bull Fish Res Bd Can 190:1–158

Webb PW (1986) Kinematics of lake sturgeon, *Acipenser fulvescens*, at cruising speeds. Can J Zool 64:2137–2141

Weihs D, Webb PW (1983) Optimization of locomotion. In: Webb PW, Weihs D (eds) Fish biomechanics. Praeger, New York, pp 339–371

Williams TL, Bowtell G, Curtin NA (1998) Predicting force generation by lamprey muscle during applied sinusoidal movement using a simple dynamic model. J Exp Biol 201:869–875

Wu T (1977) Introduction to the scaling of aquatic animal locomotion. In: Scale effects in animal locomotion. Academic Press, New York, pp 203–232